Numerical study of harbor oscillations induced by water surface disturbances within harbors of constant depth

Junliang Gao[1, 2], Xiaojun Zhou[1], Li Zhou[1 *], Jun Zang[2], Qiang Chen[2], Haoyu Ding[2]

1 School of Naval Architecture and Ocean Engineering, Jiangsu University of Science and Technology, Zhenjiang 212003, China

2. Research Unit for Water, Environment and Infrastructure Resilience (WEIR), Department of Architecture and Civil Engineering, University of Bath, BA2 7AY, U.K.

Abstract

Oscillations within an enclosed rectangular harbor and a set of partially opened rectangular harbors with various widths and locations of entrance induced by cubic water surface disturbances with different initial heights and locations are simulated using FUNWAVE 2.0 model. The height and the location of the cubic water surface disturbance refer to its thickness and its relative horizontal position inside the harbor, respectively. The water depth inside and outside all harbors is set to be constant. The aim of this paper is to investigate how different heights and locations of the water surface disturbance and various widths and locations of harbor entrance affect the oscillations inside the harbor. Results shows that for the given harbors and the range of the initial height of water surface disturbance studied in this paper, all the response amplitudes of various eigenfrequencies increase linearly with the initial height of water surface disturbance. The variations of the initial location of water surface disturbance along the backwall and sidewall of the harbor can significantly change the transverse and longitudinal oscillation patterns of various modes, respectively. The effects of the variations of the width and location of the harbor entrance on the response amplitudes of various resonant modes both depend on the relative positions of their node lines and antinode lines to the harbor entrance.

Key words:

Harbor oscillations; Resonance; Wave generation; Numerical experiments; Boussinesq equations; FUNWAVE 2.0 model

* Corresponding author. E-mail: zhouli209@hotmail.com (L. Zhou).

1. Introduction

Harbor resonance is the phenomenon of trapping and amplifying of wave energy inside a water body with a certain plane area, such as a bay or a harbor. A variety of dynamic forcings can induce significant oscillations within a harbor, which include tsunamis originating from distant earthquakes, short wave groups, infragravity waves, atmospheric fluctuations, shear flow travelling into bays or harbors and impact waves induced by submarine landslides or failures of structures near the harbor (Bellotti et al., 2012; Bowers, 1977; De Jong and Battjes, 2004; Dong et al., 2010a, b; Fabrikant, 1995; Gao et al., 2016a; Gao et al., 2017a; Okihiro and Guza, 1996).

By generating unacceptable vessel movements, harbor oscillations may interrupt the dock operations and create excessive mooring forces that may break mooring lines (López and Iglesias, 2014). Many harbors in the world have been suffering the detrimental effects caused by harbor oscillations, such as Gijón harbor in Spain (González-Marco et al., 2008), Hua-Lien harbor in Taiwan (Chen et al., 2004), Port of Long Beach in California (Kofoed-Hansen et al., 2005), Pohang New Harbor in South Korea (Kumar et al., 2014; Kumar et al., 2016) and Paradip Port in India (Kumar and Gulshan, 2017). Hence, further investigations on hydrodynamic phenomena associated with harbor oscillations have great significance in both engineering application and scientific research.

Although research efforts on harbor oscillations began in the early 1950s (Vanoni and Carr, 1950), the majority of past studies have been restricted to the stationary or the transient oscillations induced by external forcings coming from open sea. The stationary harbor oscillations are mainly excited by the periodic forcing waves such as short wave groups and infragravity waves. Oscillations within the harbor increase significantly before the energy input from the external source is balanced by losses owing to frictions, boundary absorption and radiation from the entrance (Chen et al., 2006; Gao et al., 2017b; Gao et al., 2017c; Gao et al., 2018b; Girolamo, 1996; Losada et al., 2008; Mei and Agnon, 1989; Wang et al., 2011a; Wang et al., 2015; Wang et al., 2014). The transient oscillations inside bays or harbors are mainly induced by transient long waves such as tsunami waves. When the transient long waves impinge on the harbor, the oscillations may not experience the growing stage and attain their maximum value immediately (Dong et al., 2010b; Gao et al., 2017a; Gao et al., 2016b; Gao et al., 2018a; Gao et al., 2016c).

However, investigations of harbor resonance excited by various external forcings occurring

inside bays or harbors started relatively late and few researchers focused on this problem, overall. Kulikov et al. (1996) reported that the tsunami of November 3, 1994 in Skagway, Alaska, was generated by an underwater landslide which was formed during the collapse of a cruise ship wharf undergoing construction. The tsunami caused the persistent wave motions with an amplitude of 1 m and a period of 3 min in Skagway harbor. By using a single wave inputted to the basin as an initial impulse, Yalciner and Pelinovsky (2007) proposed a short cut numerical method for evaluation of the modes of free oscillations of the basins. However, Yalciner and Pelinovsky (2007) did not systematically investigate the influences of different locations and strengths of the initial impulse on oscillation patterns. Subsequently, to understand the influence of submarine landslides on wave conditions inside bays and harbors, Wang et al. (2011a) developed a Boussinesq-type numerical model which can simulate wave generation by seafloor movement, and then studied the effects of variations of the moveable seafloor's maximum displacement, location and its velocity on the oscillation pattern systematically. It was found that small-scale seafloor movement usually induced evident larger transverse oscillations, and these transverse oscillations were sensitive to the location of the moveable seafloor. Similarly to Wang et al. (2011b), Shao et al. (2016) and Shao et al. (2017) investigated the harbor oscillations induced by water surface disturbances and submerged landslides inside rectangular harbors with parabolic bottom and constant slope bottom, respectively, and similar results were also found. However, in all these three papers, there were always two preconditions in their studies. First, the bathymetry inside the harbor must have a shape of certain type of slope (i.e., constant slope or parabolic slope). Second, all the harbors they adopted always had fully opened entrances, and the enclosed harbor or the harbors with partially opened entrances were not considered in their papers. It is still unknown whether their study findings are also valid for harbors with constant depth and for harbors with enclosed or partially opened entrances. Besides, the effects of the width and location of harbor entrance on harbor oscillations were not studied in their papers.

To further improve the knowledge of the harbor resonance induced by external forcings occurring inside the harbor, this paper systematically investigates the influences of different initial strengths and locations of water surface disturbance and various widths and locations of harbor entrance on the oscillations inside the harbor. Different from Wang et al. (2011b), Shao et al. (2016) and Shao et al. (2017), two different types of rectangular harbors (i.e. the enclosed harbor and the

partially opened harbor) with constant depth are investigated in current paper. All simulations are based on a fully nonlinear Boussinesq model, FUNWAVE 2.0, which was first proposed by Kirby et al. (2003).

The remainder of the paper is organized as follows: Section 2 briefly describes the numerical model. Section 3 introduces the numerical experiment setup. Section 4 presents the validation of oscillations within the enclosed rectangular harbor of constant depth. Section 5 demonstrates the simulation results, which are explained in detail. Concluding remarks based on the results are given in Section 6.

2. Brief description of the numerical model

All numerical experiments in this paper are performed using the famous and widespread FUNWAVE 2.0 model (Kirby et al., 2003), which is a fully nonlinear Boussinesq wave model on curvilinear coordinates. The FUNWAVE 2.0 model retains information to $O[(kh)^2]$ for frequency dispersion and to all orders for nonlinearity a/h (where k denotes the wavenumber scale, h denotes the water depth and a denotes the wave amplitude). Different types of wave-making methods can be chosen in the model. The one-way wave maker theory proposed by Chawla and Kirby (2000) is used to generate monochromatic or random waves. Solitary waves can be generated by a two-way wave maker theory. Waves can also be generated by setting the initial values of the free water surface elevation; under this condition, the wave generation becomes a pure initial value problem, and no forcing term is added in the governing equations of the model. Sponge layers are placed at the boundaries of the computational domain to effectively dissipate the energy of outgoing waves with various directions and frequencies. The capability of the model to predict wave propagation and transformation from deep to shallow water has been well validated by laboratory experiments (Kirby et al., 2003; Ma et al., 2017).

To verify the ability of the FUNWAVE 2.0 model to simulate harbor oscillations inside the harbor, Gao et al. (2016b) utilized the model to reproduce the physical experiments implemented by Rogers and Mei (1978). Gao et al. (2016b) compared the numerical results of the first three super harmonics with the experimental data of Rogers and Mei (1978) for two elongated rectangular bays of different lengths. Overall agreement was observed between the measured and the numerical results for all the three super harmonics, which indicates that the FUNWAVE 2.0 model can accurately reproduce the oscillation phenomenon inside the harbor.

3. Numerical experimental setup

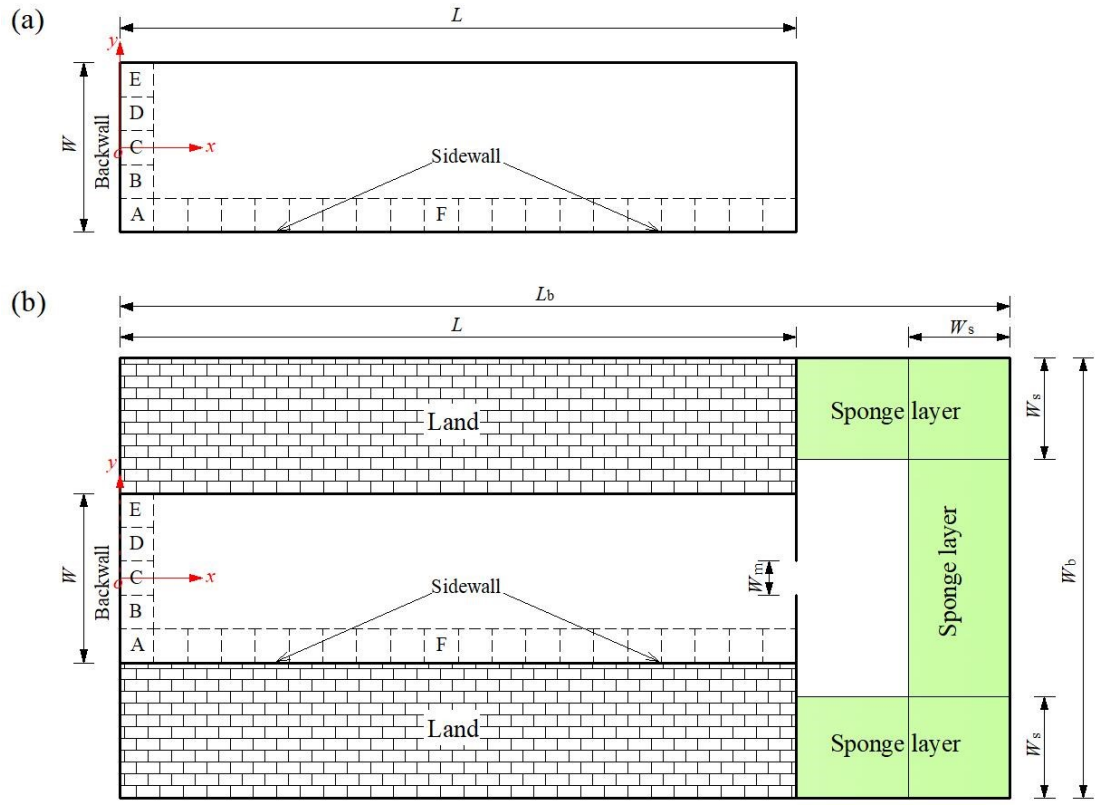

Fig. 1. Sketches of the numerical experimental setups for (a) the enclosed rectangular harbor and (b) the partially opened rectangular harbor. The square regions enclosed by dashed lines refer to different initial locations of water surface disturbances with cubic shapes.

A series of numerical experiments are carried out to investigate the oscillations inside harbors of constant depth induced by water surface disturbance occurring inside the harbor. Two different types of rectangular harbors (i.e., the enclosed rectangular harbor and the partially opened rectangular harbor) are considered in numerical experiments. Fig. 1 illustrates the sketches of the numerical experimental setups for these two types of harbors. For the enclosed rectangular harbor (Fig. 1a), it has the length of L=100.0 m and the width of W=25.0 m. The depth inside the harbor is a constant, h=3.0 m. Due to that there is no land area existing in the computational domain, the plane sizes of the numerical wave tank (NWT) are identical to these of the enclosed rectangular harbor. For the partially opened rectangular harbor (Fig. 1b), the plane sizes of the partially opened harbor are also identical to these of the enclosed harbor shown in Fig. 1a. However, because there exist land areas inside the computational domain, the plane sizes of the NWT for the partially opened

harbor are much larger than these of the harbor itself. The NWT for the partially opened harbor has a length of L_b=130.0 m and a width of W_b=65.0 m. The water depth both inside and outside the harbor is a constant and also equals h=3.0 m. All the edges of the wave tank and the harbor are set to be vertical walls with perfect reflectivity. At the right, upper and bottom boundaries of the NWT, sponge layers are arranged to dissipate the energy of radiated waves, and the width of the sponge layers is set to W_s=15.0 m. For both the two NWTs shown in Fig. 1, the origin of the Cartesian coordinate system (o, x, y, z) is placed at the center of the left boundary (backwall) of the harbor and at the still water level with z measured upwards. In all simulations, the cubic water surfaces with various heights are adopted as the initial water surface disturbances, and all the cubic disturbances have the same plane sizes of 5.0 m × 5.0 m.

As has been mentioned in the Introduction, the purpose of this paper is to investigate the influences of the following four factors on the oscillations within harbors of constant depth. These four factors include: (1) the initial strength of water surface disturbance, (2) the initial location of water surface disturbance, (3) the width of harbor entrance, and (4) the location of harbor entrance. All the numerical experiments are designed in accordance with these four variable factors. Firstly, to investigate the effects of different initial strengths of the water surface disturbance, the initial height of the cubic water surface disturbance, A_0, at the region $0 \le x \le 5.0$ m and $-12.5 \le y \le -7.5$ m (marked as A in Fig. 1) increases gradually from 0.05 m to 0.3 m in interval of 0.05 m for both the enclosed and the partially opened rectangular harbors. Secondly, to study the influences of different initial locations of the water surface disturbance, 4 more regions (i.e., B−E) of the water surface disturbance along the backwall (x=0, $-12.5 \le y \le 12.5$ m) and 19 more regions along the sidewall ($0 \le x \le 100.0$ m, $y = -12.5$ m) are also considered. However, different from the disturbance at region A, for the disturbances at these 23 regions, only the condition of A_0=0.3 m is considered. The central coordinate of the water surface disturbance in the x-y plane is denoted by (x_c, y_c). Thirdly, to discuss the effects of the width of harbor entrance, for the partially opened harbor, two different entrance widths (i.e., W_m= 2.5 m and 5.0 m) are considered, and their central coordinates are both set to (x_m, y_m) = (100.0 m, 0). Besides, the enclosed rectangular harbor is regarded as a special case of the partially opened rectangular harbor with the entrance width W_m=0. Finally, to investigate the influences of different locations of harbor entrance, for the harbor entrance with the width W_m=5.0 m, four more entrance locations are considered. For these four entrance locations, the abscissa

values of their centers are all kept to x_m=100.0 m; however, the ordinate values of their centers are different, which are equal to y_m= −10.0, −5.0, 5.0 and 10.0 m, respectively. To facilitate the reader's understanding of this article, all the parameters related to the numerical experimental setup and their physical meanings and magnitudes are presented in Table 1. In all simulations, a grid size of Δx=Δy=0.5 m and a time step of Δt=0.03 s are adopted. The total simulation time is 2,100.0 s.

Table 1. Physical meanings and magnitudes of all the parameters associated with the numerical experimental setup

Parameter	Physical meaning	Magnitude (m)
(o, x, y, z)	Cartesian coordinate system	-
A−F	Various initial locations of cubic water surface disturbance	-
A_0	Initial height of cubic water surface disturbance	For the region A: 0.05, 0.1, 0.15, 0.2, 0.25, 0.3; for other 23 regions: 0.3
h	Still water depth	3.0
L	Harbor length	100.0
L_b	Length of the NWT for the partially opened harbor	130.0
x_c	Abscissa value of the center of cubic water surface disturbance	Increasing from 2.5 to 97.5, in interval of 5.0
x_m	Abscissa value of the center of harbor entrance	100.0
y_c	Ordinate value of the center of cubic surface disturbance	−10.0, −5.0, 0, 5.0, 10.0
y_m	Ordinate value of the center of harbor entrance	For harbor with W_m=2.5 m: 0; for harbor with W_m=5.0 m: −10.0, −5.0, 0, 5.0, 10.0
W	Harbor width	25.0
W_b	Width of the NWT for the partially opened harbor	65.0
W_m	Width of entrance for the partially opened harbor	2.5, 5.0
W_s	Width of the sponge layer	15.0

All the oscillation components inside the harbor are revealed by the amplitude spectra at the corner (0, −12.5 m). For the two-dimensional oscillation problem, the resonant mode is customarily expressed as (m, n), where m and n denote the numbers of node lines parallel to the y-axis and x-

axis, respectively. Whether the oscillation component is the purely longitudinal or the purely transverse oscillation or the combination of the longitudinal and transverse oscillations can be further revealed from its spatial structure. For the purely longitudinal oscillation, there is no amplitude variation along the *y*-axis and the motions vary only along the *x*-axis; under this case, $m\neq0$ and $n=0$. Similarly, for the purely transverse oscillation, there is no amplitude variation along the *x*-axis and the motions vary only along the *y*-axis; under this case, $m=0$ and $n\neq0$. While for the combined-type oscillation, there are amplitude variations along both the *x*-axis and the *y*-axis; under this case, $m\neq0$ and $n\neq0$. The spatial variation of each component along the sidewall is used to identify the value of *m* corresponding to mode (*m*, *n*), and the spatial variation of each component along the backwall is used to identify the value of *n*. Hence, 51 wave gauges are equidistantly arranged along the sidewall; the distance between adjacent gauges is equal to 2.0 m. Meanwhile, 25 more wave gauges are equidistantly deployed along the backwall; the distance between adjacent gauges is equal to 1.0 m.

4. Validation of oscillations within enclosed rectangular harbor of constant depth

To the best of the authors' knowledge, it is the first time to use the cubic water surface distribution to investigate the resonant phenomenon within the harbor of constant depth. To verify the proposed method in predicting the eigenfrequencies of the harbor and the corresponding modal shapes, it is necessary to first introduce the analytical solution of oscillations. Due to the simplicity of the wave analysis, only analytical solution of oscillations within the enclosed rectangular harbor is introduced. It should be noted that although in theory the eigenfrequencies and the modal shapes of the partially opened rectangular harbor shown in Fig. 1b are different from those of the enclosed harbor shown in Fig. 1a, due to the relatively small entrance width studied in this paper (i.e., $W_m/W \leq 0.2$), the eigenfrequencies and the modal shapes of the former are very similar to those of the latter, which will be elaborated below.

Based on the assumptions of linear waves and shallow water, the analytical solution of oscillations within the enclosed rectangular harbor of constant depth (referring to Fig. 1a) can be expressed as following (Mei, 1983):

$$f_A = k\sqrt{gh}/2\pi \tag{1}$$

and

$$Z_{\mathrm{A}} = A\cos\frac{m\pi x}{L}\cos\frac{n\pi\left(y+W/2\right)}{W}, \tag{2}$$

where

$$k = \sqrt{\left(m\pi/L\right)^2 + \left(n\pi/W\right)^2}, \tag{3}$$

and A, f_{A} and Z_{A} denote the response amplitude, the eigenfrequency and the modal shape of mode (m, n), respectively. It is obvious that, due to the assumption of the shallow water, Eq. (1) is only valid for the resonant modes with relatively lower eigenfrequencies, and it cannot accurately predict the modes with larger eigenfrequencies. Therefore, in order to formulate the eigenfrequencies of the harbor more accurately, in this paper, the influence of the wave dispersion is taken into consideration, and the analytical eigenfrequencies of various resonant modes can be re-expressed as

$$f_{\mathrm{A}} = \sqrt{gk\tanh\left(kh\right)}\Big/2\pi. \tag{4}$$

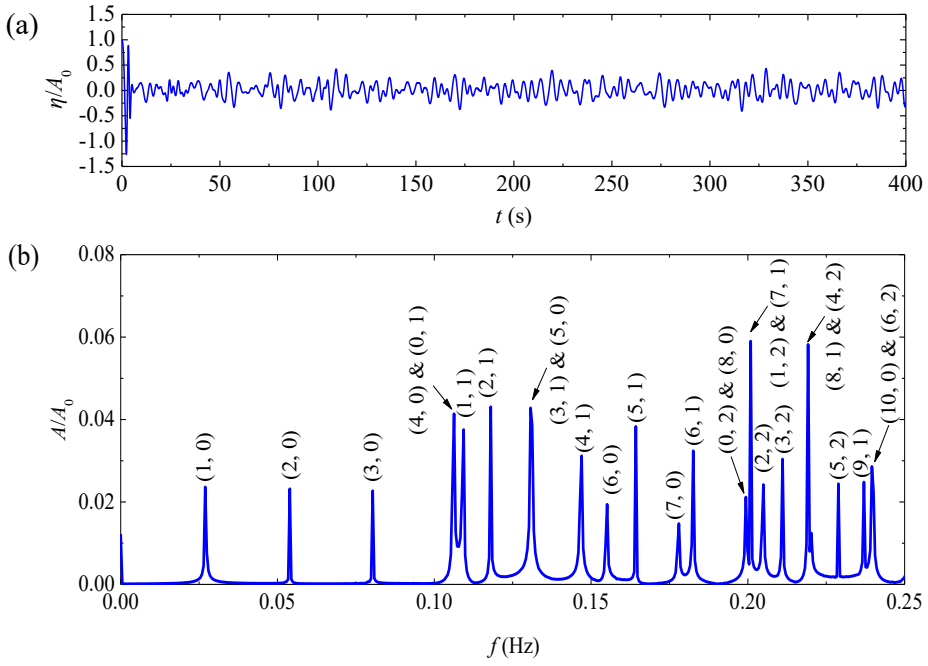

Fig. 2. (a) The time series and (b) the corresponding amplitude spectrum of the free surface elevation at the corner (0, −12.5 m) generated by the water surface disturbance with A_0=0.05 m at the region A for the enclosed rectangular harbor.

Fig. 2 demonstrates the time series and the corresponding amplitude spectrum of the free

surface elevation at the corner (0, −12.5 m) of the enclosed rectangular harbor which is excited by the water surface disturbance with A_0=0.05 m at the region A. It is noted here that although the total simulation time is 2100.0 s, only the first 400.0 s time series of the free surface elevation are presented in this figure. For the time series of the free surface elevation (Fig. 2a), at the beginning of the simulation, the fluctuation of the free surface elevation appears fairly dramatic; the relative free surface elevation, η/A_0, at the corner (0, −12.5 m) drops dramatically from 1.0 to around −1.25, and then rises sharply up to around 0.8. At about t=100.0 s, the free surface elevation remains relatively steady until the end of the simulations. Therefore, the spectral analysis of the time series of the free surface elevation is carried out with the time segment of 133.95–2,100.0 s (time interval Δt=0.03 s, hence the total number of temporal points = 2^{16}). Via the amplitude spectrum (Fig. 2b), the lowest twenty eigenfrequencies of the enclosed rectangular harbor can be numerically obtained. The resonant mode(s) that each of these eigenfrequencies corresponds to is/are also marked in the figure. It can be seen that for most of eigenfrequencies (e.g., the lowest three eigenfrequencies), each of them corresponds to only one resonant mode; while for some eigenfrequencies (i.e., the 4th, 7th, 13th, 14th, 17th and 20th eigenfrequencies), each of them corresponds to two different resonant modes. Table 2 compares the analytical and the numerical results of the lowest twenty eigenfrequencies for the enclosed harbor shown in Fig. 1a. f_N and *Err* in this table denote the numerical eigenfrequencies and their percentage errors relative to f_A, respectively. It can be found that all the values of *Err* for these twenty eigenfrequencies are less than 1.0%, which indicates fairly good agreement between the numerical and the analytical results.

Table 2. The analytical and the numerical results of the lowest twenty eigenfrequencies and the corresponding response amplitudes measured at the corner (0, −12.5 m) for the enclosed rectangular

harbor shown in Fig. 1a. f_A, f_N and *Err* refer to the analytical eigenfrequency, the numerical eigenfrequency and the percentage error between them, respectively, and A_N denotes the response amplitude measured from the simulation.

No.	Mode (m, n)	f_A (Hz)	f_N (Hz)	*Err* (%)	A_N/A_0
1	(1, 0)	0.0270	0.0271	0.3704	0.0236
2	(2, 0)	0.0539	0.0539	0	0.0232
3	(3, 0)	0.0804	0.0803	0.1244	0.0227
4	(4, 0) & (0, 1)	0.1063	0.1060	0.2822	0.0414
5	(1, 1)	0.1094	0.1091	0.2742	0.0376
6	(2, 1)	0.1180	0.1178	0.1695	0.0430
7	(5, 0) & (3, 1)	0.1312	0.1309	0.2287	0.0428
8	(4, 1)	0.1450	0.1463	0.8966	0.0314
9	(6, 0)	0.1551	0.1548	0.1934	0.0194
10	(5, 1)	0.1643	0.1641	0.1217	0.0383
11	(7, 0)	0.1780	0.1777	0.1685	0.0147
12	(6, 1)	0.1826	0.1823	0.1643	0.0324
13	(8, 0) & (0, 2)	0.1999	0.1994	0.2501	0.0212
14	(7, 1) & (1, 2)	0.2009	0.2008	0.0498	0.059
15	(2, 2)	0.2050	0.2046	0.1951	0.0242
16	(3, 2)	0.2111	0.2108	0.1421	0.0304
17	(8, 1) & (4, 2)	0.2192	0.2190	0.0912	0.0582
18	(5, 2)	0.2289	0.2287	0.0874	0.0244
19	(9, 1)	0.2370	0.2368	0.0844	0.0248
20	(10, 0) & (6, 2)	0.2401	0.2396	0.2082	0.0286

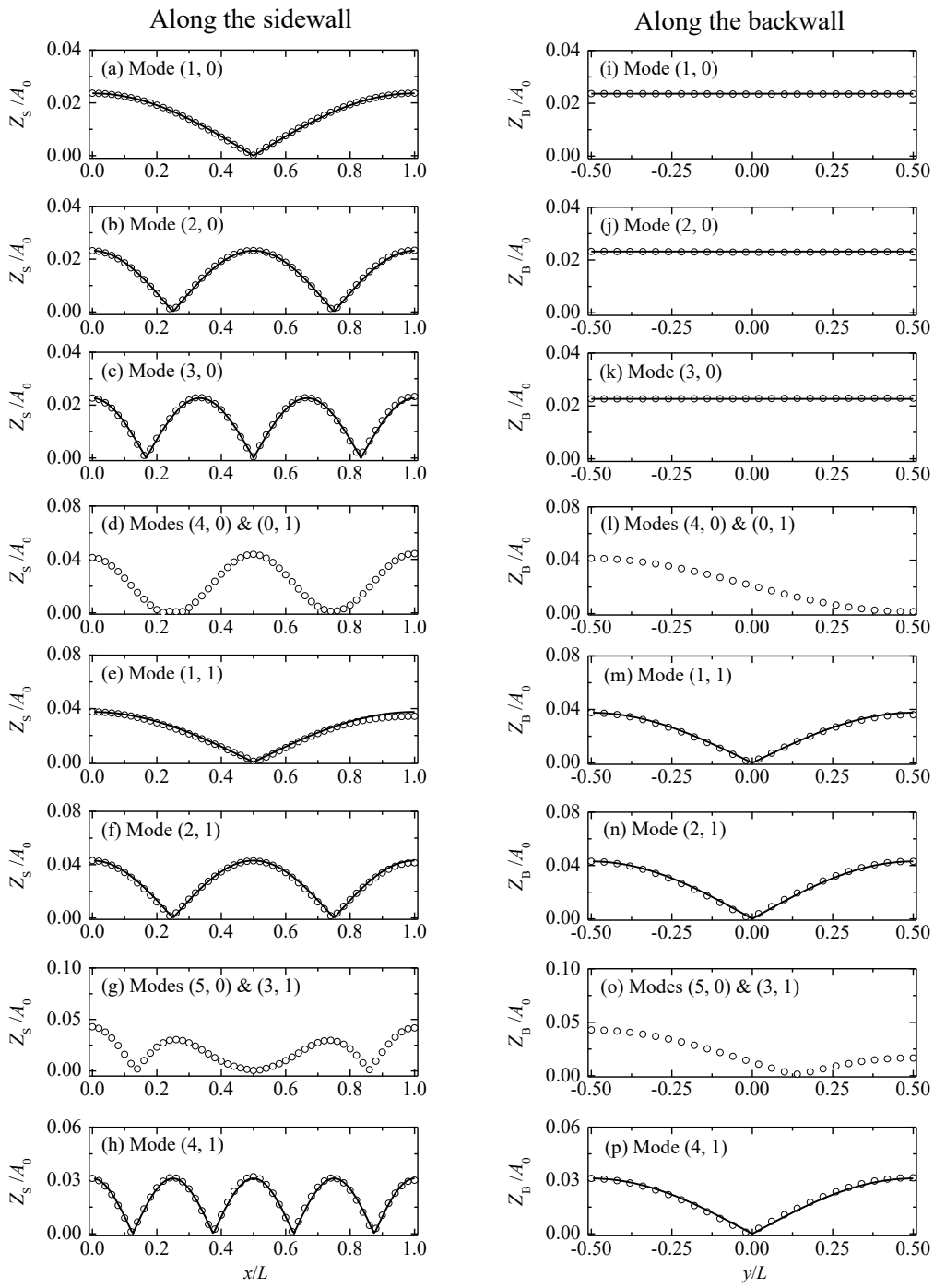

Fig. 3. The analytical (solid lines) and the numerical (dots) oscillation profiles for the lowest eight eigenfrequencies of the enclosed harbor. (a)–(h) and (i)–(p) correspond to the oscillation profiles along the sidewall and along the backwall, respectively. Oscillations inside the harbor are induced by the water surface disturbance with A_0=0.05 m at the region A.

Fig. 3 compares the analytical and the numerical oscillation profiles along the sidewall and the backwall of the enclosed rectangular harbor for the lowest eight eigenfrequencies. Z_S and Z_B in the

figure denote the oscillation profiles along the sidewall and along the backwall, respectively. Based on the analytical resonant modal shapes inside the enclosed rectangular harbor, Eq. (2), the analytical expressions of Z_S and Z_B for mode (m, n) can be easily formulated by

$$Z_S = |Z_A(x, y = -W/2)| = \left| A\cos\frac{m\pi x}{L} \right|, \tag{5}$$

and

$$Z_B = |Z_A(x = 0, y)| = \left| A\cos\frac{n\pi(y + W/2)}{W} \right|, \tag{6}$$

respectively. It should be noted here that for the 4th and the 7th eigenfrequencies, due to that each of their resonant modal shapes inside the harbor is modulated by two different resonant modes, there exists no analytical oscillation profile. Hence, for the two eigenfrequencies, only the numerical oscillation profiles along the sidewall and the backwall are presented in this figure. For the other 6 eigenfrequencies, fairly good agreement between the numerical and the analytical oscillation profiles along both the sidewall and the backwall of the harbor is obtained.

As mentioned before, although the eigenfrequencies and the modal shapes of the partially opened rectangular harbor shown in Fig. 1b are theoretically different from the enclosed harbor shown in Fig. 1a, due to the relatively small entrance width studied in this paper (i.e., $W_m/W \leq 0.2$), the eigenfrequencies and the modal shapes of the former are very similar to those of the latter. Table 3 presents the numerical eigenfrequencies of the lowest twenty eigenfrequencies for the two partially opened harbors with W_m=2.5 and 5.0 m and the entrance location (x_m, y_m)=(100.0 m, 0) and their percentage errors relative to those of the enclosed harbor. For both the two partially opened harbors with different entrance widths, various resonant modes are also excited by the cubic water surface disturbance with A_0=0.05 m at the region A. It can be seen that except that the lowest two eigenfrequencies seem sensitive to the width of harbor entrance, the other eighteen eigenfrequencies of the partially opened harbors are very close to the corresponding ones of the enclosed harbor. All the percentage errors of these eighteen eigenfrequencies relative to those of the enclosed harbor are approximately equal to or less than 2.0%. Fig. 4 illustrates the comparisons of the numerical oscillation profiles of the modes (3, 0), (2, 1), (6, 0) and (6, 1) for the three harbors with different entrance widths. For all the four resonant modes, overall agreement is also observed for the oscillation profiles along both the sidewall and the backwall.

Table 3. The numerical results of the lowest twenty eigenfrequencies and the corresponding response amplitudes measured at the corner (0, −12.5 m) for the partially opened harbors with W_m=2.5 and 5.0 m and (x_m, y_m)=(100.0 m, 0). $f_{N2.5}$, $f_{N5.0}$, $Err1$ and $Err2$ denote the numerical eigenfrequencies of the partially opened harbors with W_m=2.5 and 5.0 m and their percentage errors relative to f_N, respectively. $A_{2.5}$, $A_{5.0}$, $R1$ and $R2$ denote the response amplitudes at the partially opened harbors with W_m=2.5 and 5.0 m and their percentage ratios relative to A_N, respectively. The values of f_N and A_N are listed in Table 2.

No.	Mode (m, n)	$f_{N2.5}$ (Hz)	$f_{N5.0}$ (Hz)	$Err1$ (%)	$Err2$ (%)	$A_{2.5}/A_0$	$A_{5.0}/A_0$	$R1$ (%)	$R2$ (%)
1	(1, 0)	0.0300	0.0325	10.70	19.93	0.0008	0.0007	3.390	2.966
2	(2, 0)	0.0554	0.0565	2.783	4.824	0.0043	0.0038	18.53	16.38
3	(3, 0)	0.0813	0.0819	1.245	1.990	0.0062	0.0059	27.31	25.99
4	(4, 0) & (0, 1)	0.1063	0.1063	0.2830	0.2830	0.0130	0.0178	31.40	42.99
5	(1, 1)	0.1094	0.1094	0.2750	0.2750	0.0336	0.0341	89.36	90.69
6	(2, 1)	0.1180	0.1180	0.1698	0.1698	0.0416	0.036	96.74	83.72
7	(5, 0) & (3, 1)	0.1307	0.1312	0.1528	0.2291	0.0284	0.0338	66.36	78.97
8	(4, 1)	0.1470	0.1470	0.4785	0.4785	0.0305	0.0307	97.13	97.77
9	(6, 0)	0.1551	0.1556	0.1938	0.5168	0.0062	0.0031	31.96	15.98
10	(5, 1)	0.1643	0.1643	0.1218	0.1219	0.0378	0.0346	98.69	90.34
11	(7, 0)	0.1780	0.1785	0.1688	0.4502	0.0079	0.0035	53.74	23.81
12	(6, 1)	0.1826	0.1826	0.1646	0.1646	0.0322	0.0322	99.38	99.38
13	(8, 0) & (0, 2)	0.1999	0.1994	0.2508	0	0.0165	0.0168	77.83	79.24
14	(7, 1) & (1, 2)	0.2009	0.2009	0.0498	0.0498	0.0282	0.0238	47.79	40.34
15	(2, 2)	0.2055	0.2055	0.4399	0.4399	0.0074	0.0038	30.58	15.70
16	(3, 2)	0.2116	0.2116	0.3795	0.3795	0.0076	0.0033	25.00	10.86
17	(8, 1) & (4, 2)	0.2192	0.2192	0.0913	0.0913	0.029	0.027	49.83	46.39
18	(5, 2)	0.2294	0.2294	0.3061	0.3060	0.0055	0.0015	22.54	6.148
19	(9, 1)	0.2370	0.2370	0.0845	0.0845	0.0246	0.0236	99.19	95.16
20	(10, 0) & (6, 2)	0.2401	0.2401	0.2087	0.2087	0.0189	0.0254	66.08	88.81

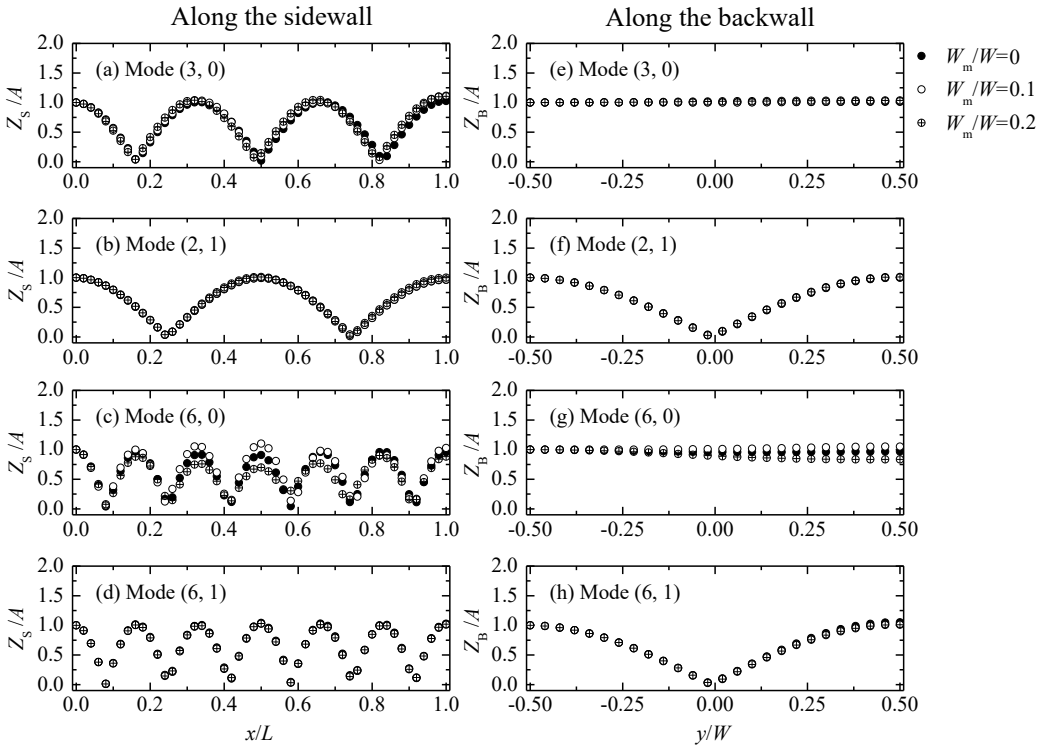

Fig. 4. Numerical oscillation profiles of the modes (3, 0), (2, 1), (6, 0) and (6, 1) for the three harbors with different entrance widths. (a)–(d) and (e)–(h) correspond to the oscillation profiles along the sidewall and the backwall, respectively. Oscillations inside all the three harbors are excited by the water surface disturbance with A_0=0.05 m at the region A.

The response amplitudes of the lowest twenty eigenfrequencies measured at the corner (0, −12.5 m) for the enclosed and the partially opened harbors are also listed in Tables 2 and 3, respectively. It can be clearly seen that due to the wave energy radiation into the open sea through the entrance, the resonant amplitudes of each eigenfrequencies inside the partially opened harbors are less than the corresponding ones inside the enclosed harbor. However, the sensitivity of different resonant modes to harbor entrance is different. For all the modes (m, n) with n=0 and n=2 [e.g., the modes (1, 0) and (2, 2)], their response amplitude decreases sharply due to the existence of harbor entrance; the larger the entrance width is, the less the response amplitude becomes. However, for all the modes (m, n) with n=1 [e.g., the mode (1, 1)], their response amplitudes seems insensitive to the variation of the entrance width. The reasons for these phenomena will be elaborated in Section 5.3.

5. Results and discussion

5.1. Effects of the initial height of water surface disturbance

Similar to Fig. 2, the spectral analyses of the time series of the free surface elevations at the cornel (0, −12.5 m) excited by the water surface disturbances with A_0=0.10−0.30 m at the region A for the enclosed harbor are also carried out. Fig. 5 shows the variations of the response amplitudes of the lowest twenty eigenfrequencies with respect to the height of the water surface disturbance, A_0. It can be easily found that at the variation range of the initial height of the water surface disturbance studied in this paper, all the response amplitudes of the lowest twenty eigenfrequencies increase linearly with the initial height of the water surface disturbance. This phenomenon may be attributed to that only small oscillations compared with the still water depth are investigated in current paper, and nonlinear energy transfers between different resonant components can be neglected.

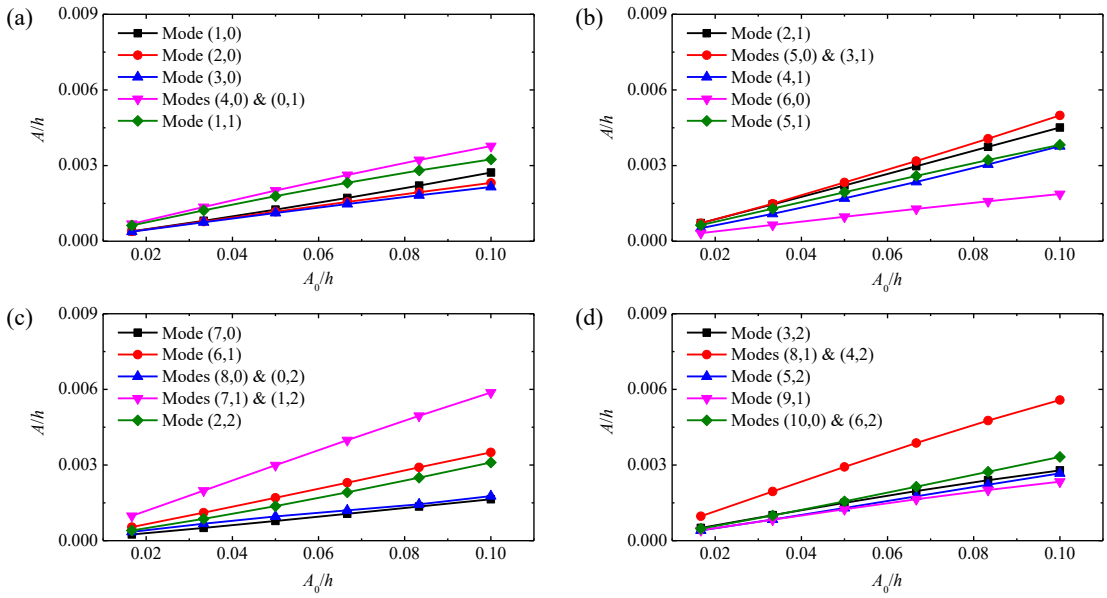

Fig. 5. Response amplitudes of the lowest twenty eigenfrequencies at the corner (0, −12.5 m) induced by the water surface disturbances with various initial heights at the region A for the enclosed rectangular harbor. (a)−(d) correspond to the response amplitudes of the 1st–5th, the 6th–10th, the 11th–15th and the 16th–20th eigenfrequencies, respectively.

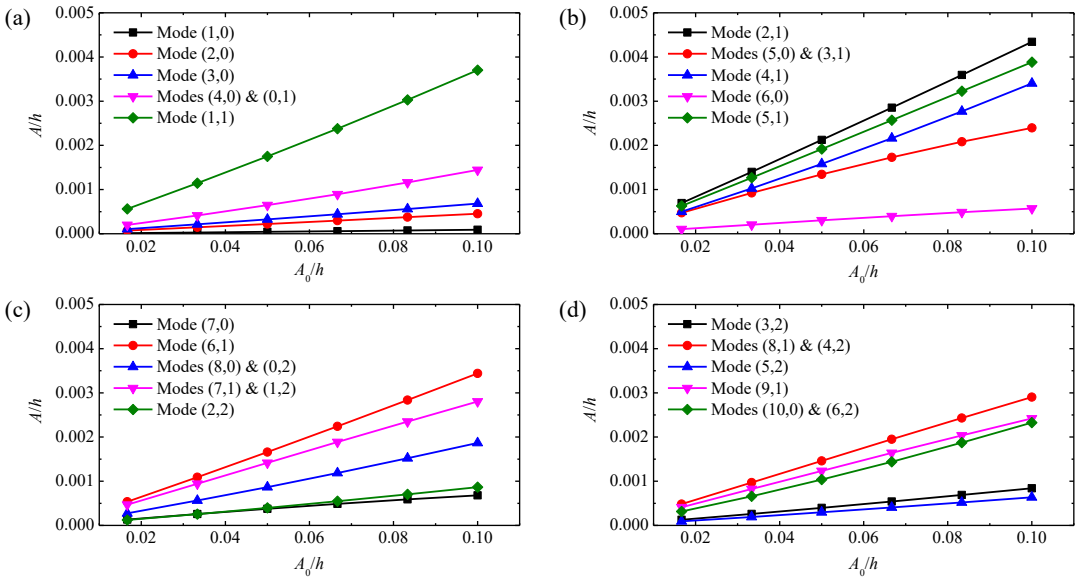

Fig. 6. Response amplitudes of the lowest twenty eigenfrequencies at the corner (0, −12.5 m) generated by the water surface disturbances with various initial heights at the region A for the partially opened rectangular harbor with W_m=2.5 m and (x_m, y_m)=(100.0 m, 0). (a)−(d) correspond to the response amplitudes of the 1st−5th, the 6th−10th, the 11th−15th and the 16th−20th eigenfrequencies, respectively.

Again, similar to Fig. 2, the spectral analyses of the time series of the free surface elevations at the cornel (0, −12.5 m) generated by the water surface disturbances with A_0=0.05−0.30 m at the region A for the two partially opened rectangular harbors with W_m=2.5 and 5.0 m and (x_m, y_m)=(100.0 m, 0) are also implemented. Fig. 6 illustrates the variations of the response amplitudes of the lowest twenty eigenfrequencies with the initial height of the water surface disturbance, A_0, for the partially opened harbor with W_m=2.5 m. Identical to Fig. 5, all the response amplitudes of these twenty eigenfrequencies for the partially opened harbor with W_m=2.5 m grow linearly with A_0. The analysis results for the partially opened harbor with W_m=5.0 m are similar to those shown in Figs. 5 and 6. Due to the limitation of space, these analysis results are not presented in this article.

5.2. Effects of the initial location of water surface disturbance

As shown in Fig. 1, there are five different initial disturbance locations along the backwall (i.e., the regions A-E) and twenty-five different initial disturbance locations along the sidewall. The effects of the variations of the disturbance location along the backwall and along the sidewall on the

oscillations are discussed one by one.

5.2.1 Water surface disturbance along the backwall

Fig. 7 shows the amplitude spectra of the time series of the free surface elevations at the corner (0, −12.5 m) excited by the water surface disturbances with A_0=0.3 m at the regions A-E for the enclosed rectangular harbor. The resonant modes that correspond to the lowest twenty eigenfrequencies are also marked in the figure. It can be intuitively observed that changing the initial location of the water surface disturbance can lead to evidently different oscillations inside the harbor. Specifically speaking, the lowest twenty eigenfrequencies can be classified into four different types. The first three types of eigenfrequencies refer to those that correspond to the modes (m, n) with n=0, n=1 and n=2, respectively, and each eigenfrequency in these three types corresponds to only one resonant mode. On the contrary, the fourth type of eigenfrequencies includes the 4th, 7th, 13th, 14th, 17th and 20th eigenfrequencies, each of which corresponds to two different modes. For the first type of eigenfrequencies, such as the lowest three eigenfrequencies corresponding to the modes (1, 0), (2, 0) and (3, 0), their response amplitudes seem insensitive to the initial location variation of the water surface disturbance along the backwall. However, for both the second and the third types of eigenfrequencies, their response amplitudes strongly depend on the relative position of the water surface disturbance to node lines or antinode lines along the backwall. For the resonant mode (m, n) with n≥1, there are n+1 antinode lines and n node lines along the backwall. When the water surface disturbance is located at one of the n node lines along the backwall, various modes related to this particular n are remarkably restrained. In contrast, when the water surface disturbance is located at one of the n+1 antinode lines, resonant modes related to n are evidently excited. Take Fig. 7c for example. For the second type of eigenfrequencies [e.g., the modes (1, 1), (2, 1) and (4, 1)], due to that the center line of the region C is superposed with their sole node line at y=0, their response amplitudes are very small. In stark contrast, for the third type of eigenfrequencies [i.e., the modes (2, 2), (3, 2) and (5, 2)], because the center line of the region C is superposed with one of their three antinode lines, all of them have very outstanding response amplitudes. Similar phenomena can also be easily observed in Fig. 7 a, b, d and e. To show these phenomena more intuitively, the variations of the response amplitudes of the first three types of eigenfrequencies with various disturbance locations along the backwall are further illustrated in Fig. 8. For the fourth type of eigenfrequencies, because each of their modal shapes is modulated by two different resonant modes, their oscillation

patterns are usually complicated and irregular (referring to Fig. 3d, g, l and o). Besides, their modal shapes may vary with the initial location of the water surface disturbance as well. Therefore, it is hard to determine the exact positions of the node lines and the antinode lines for these eigenfrequencies. Hence, based on these reasons, the effects of the location variation of the water surface disturbance on the fourth type of eigenfrequencies are not discussed in this paper.

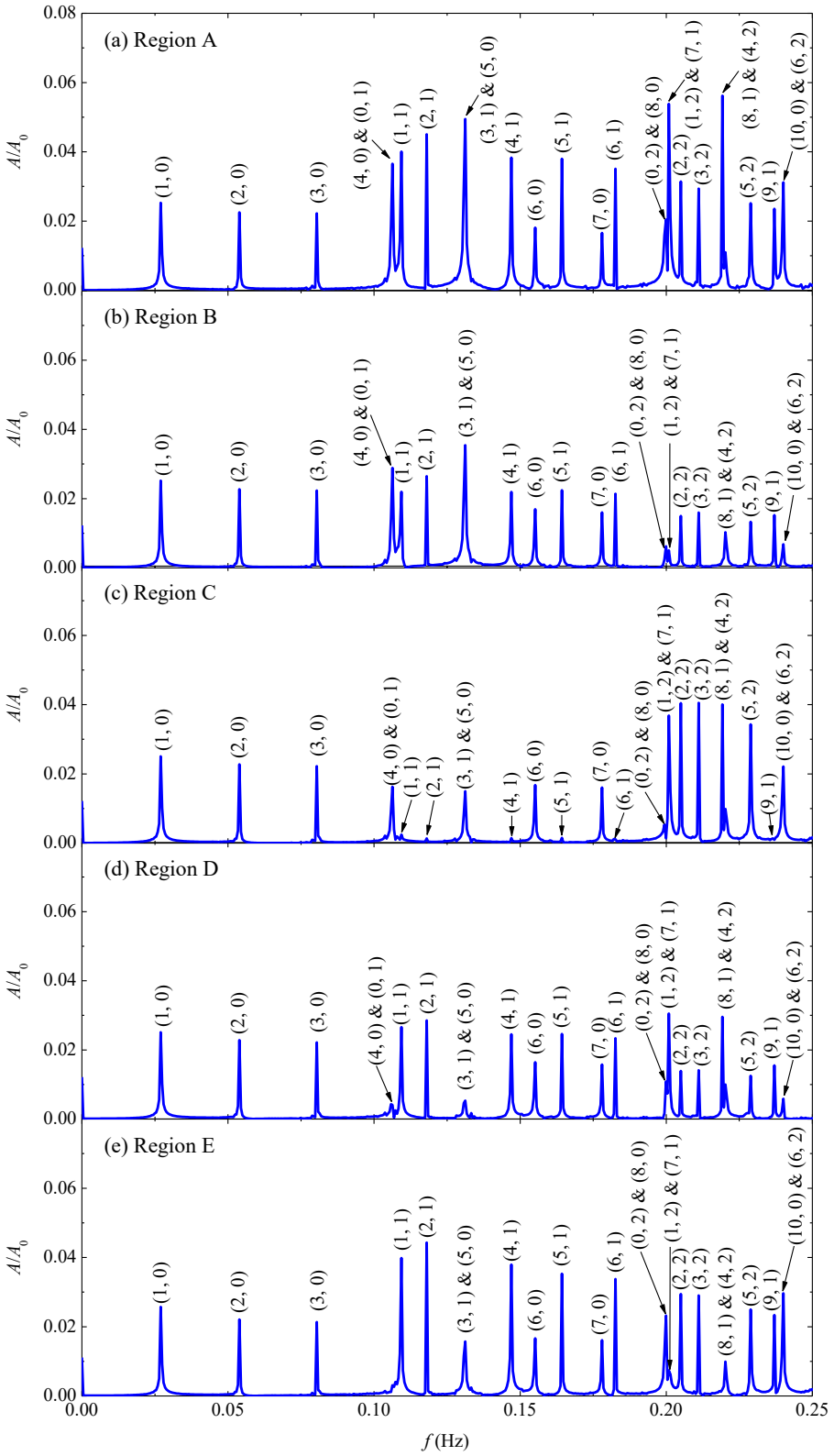

Fig. 7. Amplitude spectra of the time series of the free surface elevations at the corner (0, −12.5 m) excited by the water surface disturbances with A_0=0.3 m at the regions A-E for the enclosed rectangular harbor

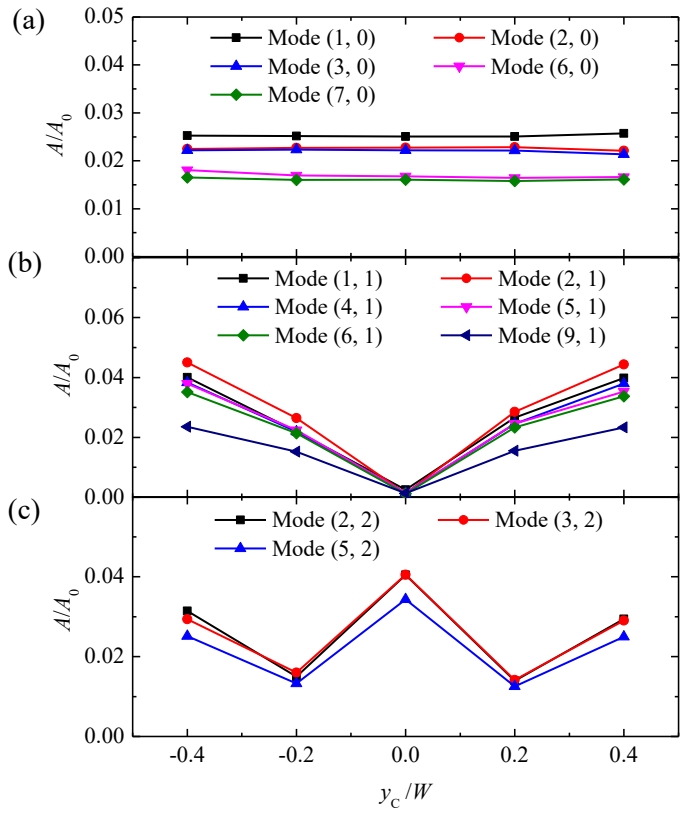

Fig. 8. Variations of the response amplitudes of different modes at the corner (0, −12.5 m) with respect to various disturbance locations along the backwall of the enclosed rectangular harbor: (a) five resonant modes with n=0; (b) six resonant modes with n=1; (c) three resonant modes with n=2

Similar to Fig. 7, Fig. 9 shows the amplitude spectra of the time series of the free surface elevations at the corner (0, −12.5 m) excited by the water surface disturbances with A_0=0.3 m at the regions A-E for the partially opened rectangular harbor with W_m=2.5 m and (x_m, y_m)=(100.0 m, 0). Although the resonance intensity inside the partially opened harbor is obviously lower than that inside the enclosed harbor due to the wave energy leakage from the entrance, all the phenomena embodied in Fig. 7 are also reflected in Fig. 9. For the first type of eigenfrequencies, their response amplitudes are insensitive to the various disturbance locations along the backwall. For the second and third types of eigenfrequencies, if the water surface disturbance was located at one of the n node lines, the modes related to n would be significantly inhibited; if it was at one of the n+1 antinode lines, the modes related to n would be evidently excited. To show these phenomena more intuitively, Fig. 10 further presents the variations of the response amplitudes of the first three types of eigenfrequencies with various disturbance locations along the backwall of the partially opened harbor.

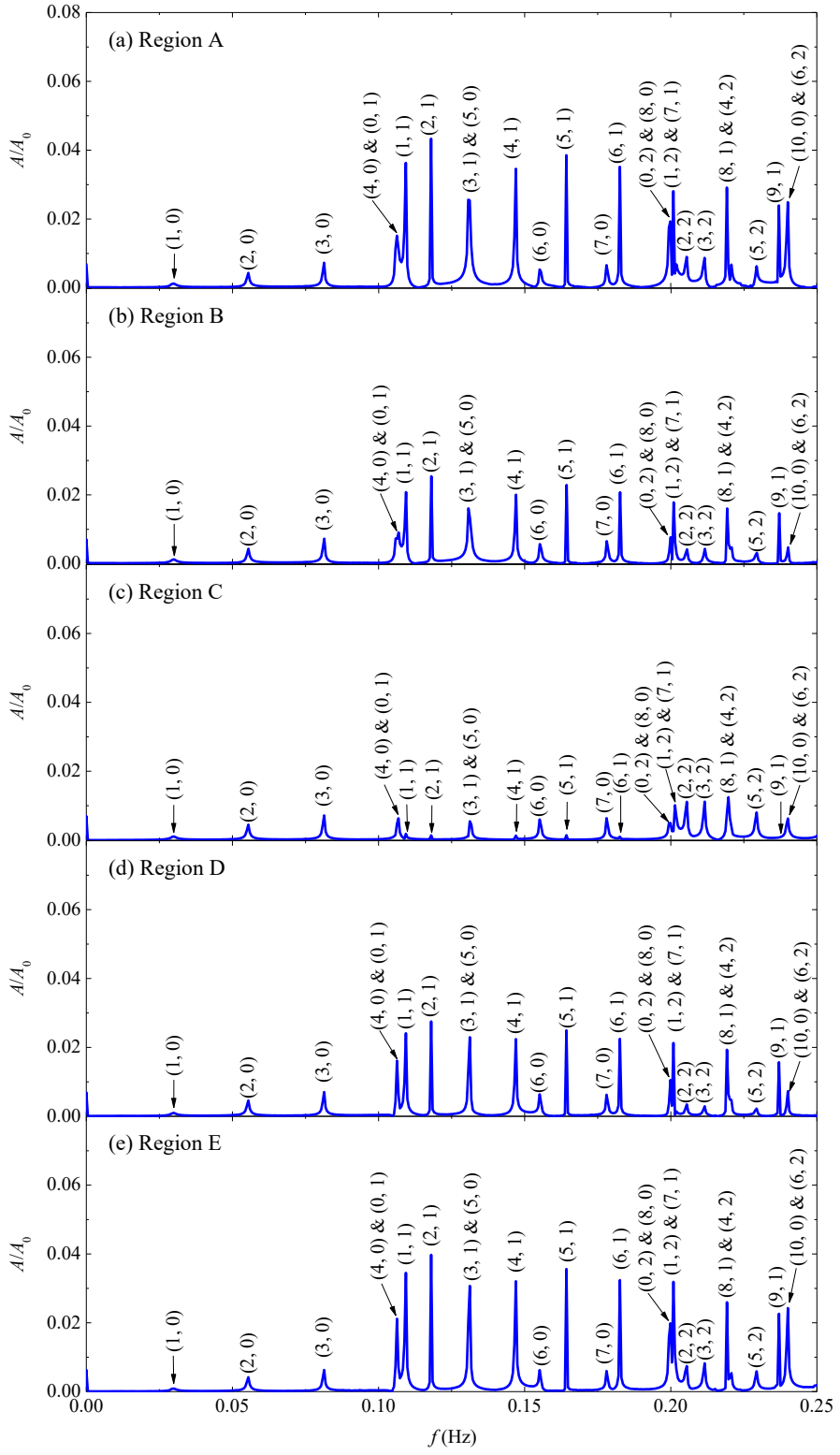

Fig. 9. Amplitude spectra of the time series of the free surface elevations at the corner (0, −12.5 m) excited by the water surface disturbances with A_0=0.3 m at the regions A-E for the partially opened rectangular harbor with W_m=2.5 m and (x_m, y_m)=(100.0 m, 0)

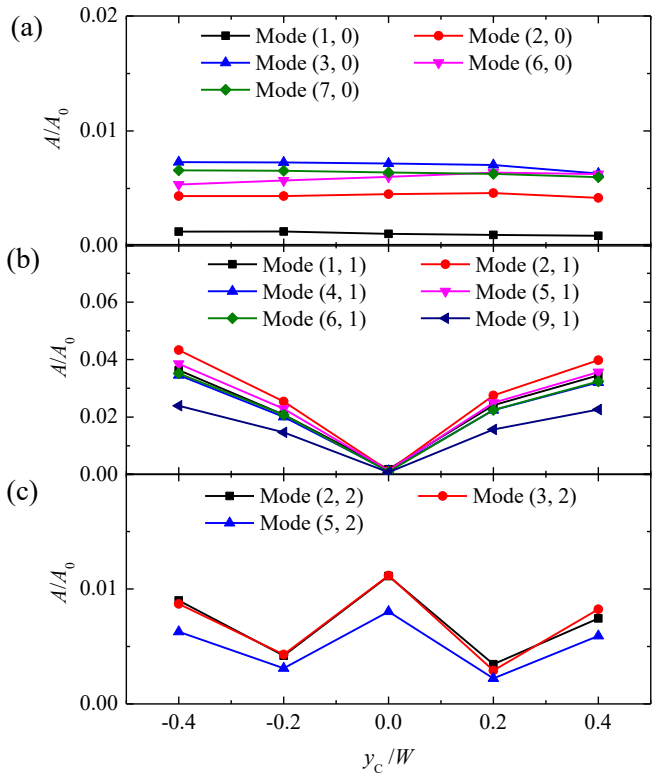

Fig. 10. Variations of the response amplitudes of different modes at the corner (0, −12.5 m) with respect to various disturbance locations along the backwall the partially opened rectangular harbor with W_m=2.5 m and (x_m, y_m)=(100.0 m, 0): (a) five resonant modes with n=0; (b) six resonant modes with n=1; (c) three resonant modes with n=2

5.2.2 Water surface disturbance along the sidewall

To study the differences between oscillations induced by the same water surface disturbance but with various offshore locations, the location of the water surface disturbance with A_0=0.3 m is shifted along the entire length of the sidewall with an increment of 5.0 m. However, results are discussed in detail only for the region F (referring to Fig. 1, 45.0 ≤ x ≤ 50.0 m and −12.5 ≤ y ≤ −7.5 m). Fig. 11 shows the amplitude spectrum of the time series of the free surface elevation at the corner (0, −12.5 m) excited by the water surface disturbance with A_0=0.3 m at the region F for the enclosed rectangular harbor. Oscillations presented in this figure are distinct from those induced by various backwall positions (referring to Fig. 7). Only a few resonant modes in this figure have response amplitudes comparable to the corresponding ones in Fig. 7, and for most of the resonant modes, their response amplitudes remarkably decrease. Take the lowest three modes, i.e. the modes (1, 0), (2, 0) and (3, 0), for example. Among the three modes, only the response amplitude of the

mode (2, 0) is similar to that shown in Fig. 7. While for the modes (1, 0) and (3, 0), both of their response amplitudes become much less. For the resonant mode (m, n) with m≥1, there are m+1 antinode lines and m node lines along the sidewall. It can be observed from Fig. 11 that, all the modes for which one of the m node lines is superposed with or very close to the center line of the region F have relatively small response amplitudes; conversely, all the modes for which one of the m+1 antinode lines is superposed with or very close to the center line of the region F are usually particularly evident.

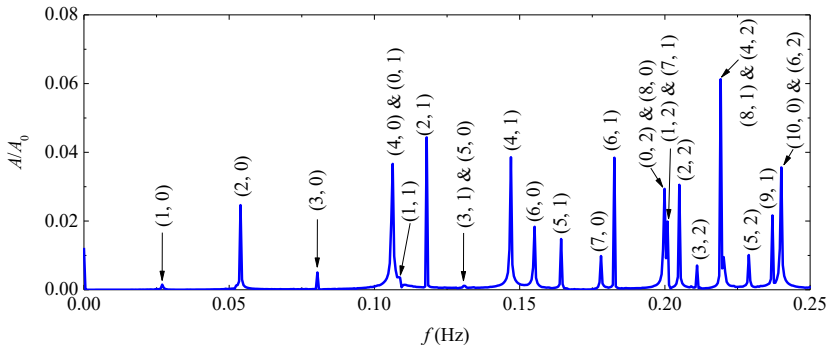

Fig. 11. Amplitude spectrum of the time series of the free surface elevation at the corner (0, −12.5 m) excited by the water surface disturbance with A_0=0.3 m at the region F for the enclosed rectangular harbor

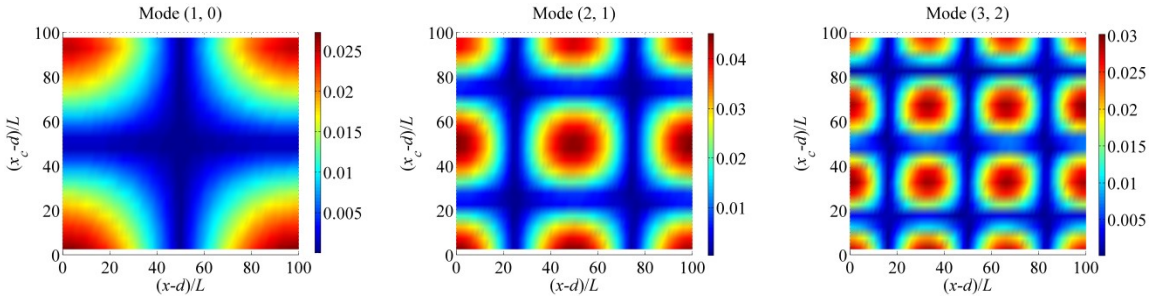

Fig. 12. Variations of the offshore oscillation profiles of the modes (1, 0), (2, 1) and (3, 2) with respect to various disturbance locations along the sidewall of the enclosed rectangular harbor. The colorbar denotes the relative amplitude A/A_0.

To further examine the above finding, Fig. 12 shows the variations of the offshore oscillation profiles of the modes (1, 0), (2, 1) and (3, 2) with respect to various disturbance locations along the sidewall of the enclosed rectangular harbor. It is seen that the longitudinal oscillation patterns of the

three modes are all closely related to the disturbance location along the sidewall. It more visually shows that when the water surface disturbance is located at one of the m+1 antinode lines, the resonant mode is evidently induced; whereas when it is located at one of the m node lines, the mode becomes extremely small.

Similar to Figs. 11 and 12, Figs. 13 and 14 show respectively the amplitude spectrum of the time series of the free surface elevation at the corner (0, −12.5 m) excited by the water surface disturbance with A_0=0.3 m at the region F and the variations of the offshore oscillation profiles of the modes (1, 0), (2, 1) and (3, 2) with respect to various disturbance locations along the sidewall for the partially opened rectangular harbor with W_m=2.5 m and (x_m, y_m)=(100.0 m, 0). All the phenomena presented in Figs. 11 and 12 also can be easily observed in these two figures.

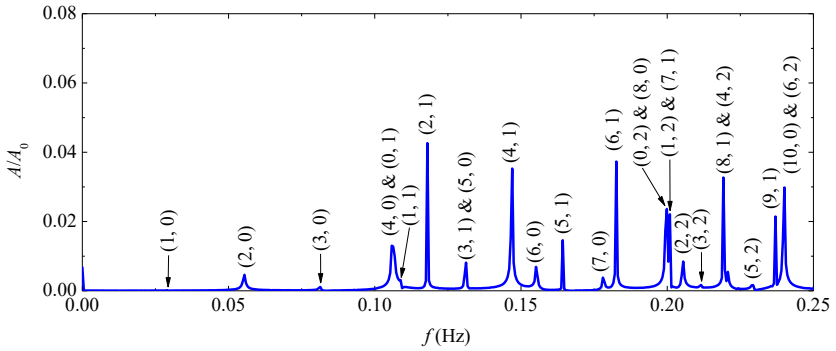

Fig. 13. Amplitude spectrum of the time series of the free surface elevation at the corner (0, −12.5 m) excited by the water surface disturbance with A_0=0.3 m at the region F for the partially opened rectangular harbor with W_m=2.5 m and (x_m, y_m)=(100.0 m, 0)

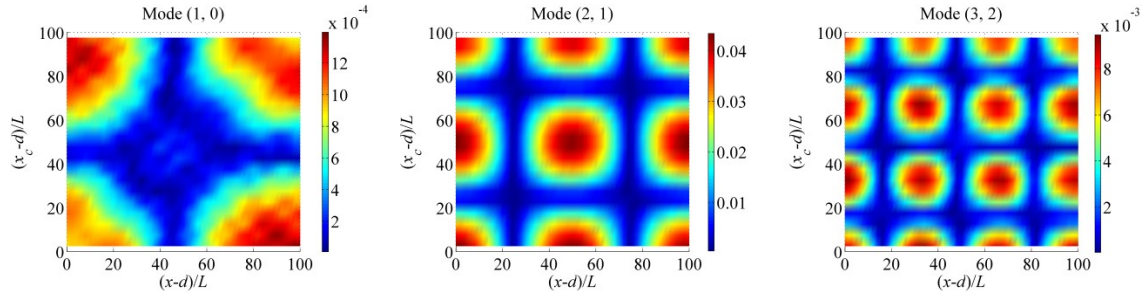

Fig.14. Variations of the offshore oscillation profiles of the modes (1, 0), (2, 1) and (3, 2) with respect to various disturbance locations along the sidewall of the partially opened rectangular harbor with W_m=2.5 m and (x_m, y_m)=(100.0 m, 0)

5.3. Effects of the width of harbor entrance

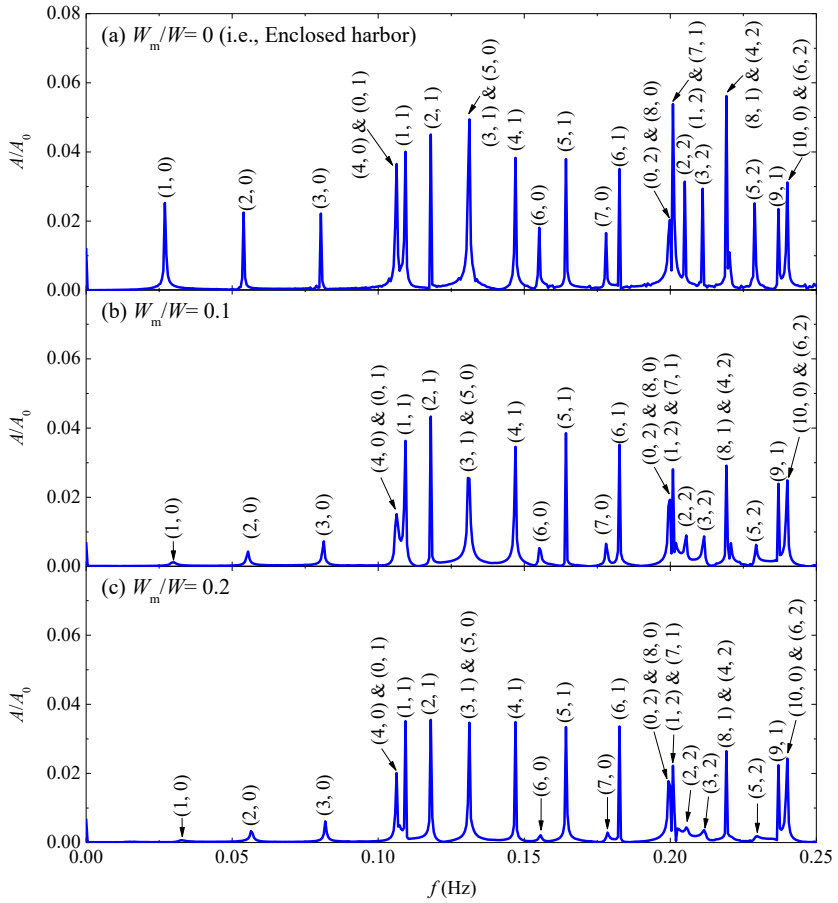

Fig. 15. Amplitude spectra of the time series of the free surface elevations at the corner (0, −12.5 m) generated by the water surface disturbance at the region A for the three harbors with different widths of harbor entrance under the conditions of A_0=0.3 m and that the center of harbor entrance is located at (100.0 m, 0).

Fig. 15 shows the amplitude spectra of the time series of the free surface elevations at the corner (0, −12.5 m) generated by the water surface disturbance at the region A for the three harbors with different entrance widths under the conditions of A_0=0.3 m and that the center of harbor entrance is located at (100.0 m, 0). As mentioned in Section 3, the enclosed rectangular harbor is regarded as a special case of the partially opened rectangular harbor with the entrance width W_m=0. It is seen that due to the wave energy leakage from the entrance, the oscillations of various eigenfrequencies inside the two partially opened harbors are less than the corresponding ones inside the enclosed harbor, overall. The larger the entrance width is, the more obvious this phenomenon

becomes. However, the influencing degrees of changing the entrance width on different modes are different. Identical to Section 5.2.1, the lowest twenty eigenfrequencies are classified into the same four types. For the first type of eigenfrequencies that correspond to the modes (m, n) with n=0, their response amplitudes decrease sharply with the increasing of the width of harbor entrance. The similar phenomenon can also be easily found for the third type of eigenfrequencies that correspond to the modes (m, n) with n=2. In contrast, for the second type of eigenfrequencies that correspond to the modes (m, n) with n=1, their response amplitudes seems insensitive to the variation of the width of harbor entrance. To show these phenomena more visually, the variation of the response amplitudes of these three types of eigenfrequencies at the corner (0, −12.5 m) with respect to the width of harbor entrance are further illustrated in Fig. 16. Identical to Section 5.2.1, the effects of changing the width of harbor entrance on the response amplitudes of the fourth types of eigenfrequencies are not discussed in this paper. It should be noted that these phenomena shown in Figs. 15 and 16 are almost identical to those embodied in Table 3 that compares the response amplitudes of the various eigenfrequencies inside the same three harbors but induced by the water surface disturbance with A_0=0.05 m.

The reason why these three types of eigenfrequencies have different sensitivity degrees for the width of harbor entrance lies on the different relative positions of their node lines and antinode lines to the harbor entrance. For the first type of eigenfrequencies, they correspond to the modes (m, n) with n=0. As mentioned in Section 3, these resonant modes are purely longitudinal oscillations. In theory, for these resonant modes inside the enclosed harbor, the oscillation amplitude along the backwall and the right wall of the harbor (x = 100.0 m; $-12.5 \leq y \leq 12.5$ m) is a constant and its magnitude is the largest inside the harbor. It means that once an entrance is opened at the right wall, there exists large difference on the wave energy levels inside and outside the entrance, and the energy of these resonant modes inside the harbor leaks into the open sea rapidly. In addition, the larger the entrance width is, the larger the radiation damping becomes. Therefore, the response amplitudes of these purely longitudinal modes decrease sharply with the increase of the width of harbor entrance. Similarly, for the third type of eigenfrequencies that correspond to the modes (m, n) with n=2, there exists an antinode line at the harbor entrance, which also causes large difference on the wave energy levels inside and outside the entrance. On the contrary, for the second type of eigenfrequencies that correspond to the modes (m, n) with n=1, there exists a node line at the harbor

entrance. The imbalance of the wave energy level for these eigenfrequencies around the harbor entrance becomes extremely small, which causes much slower wave energy leakage from the entrance.

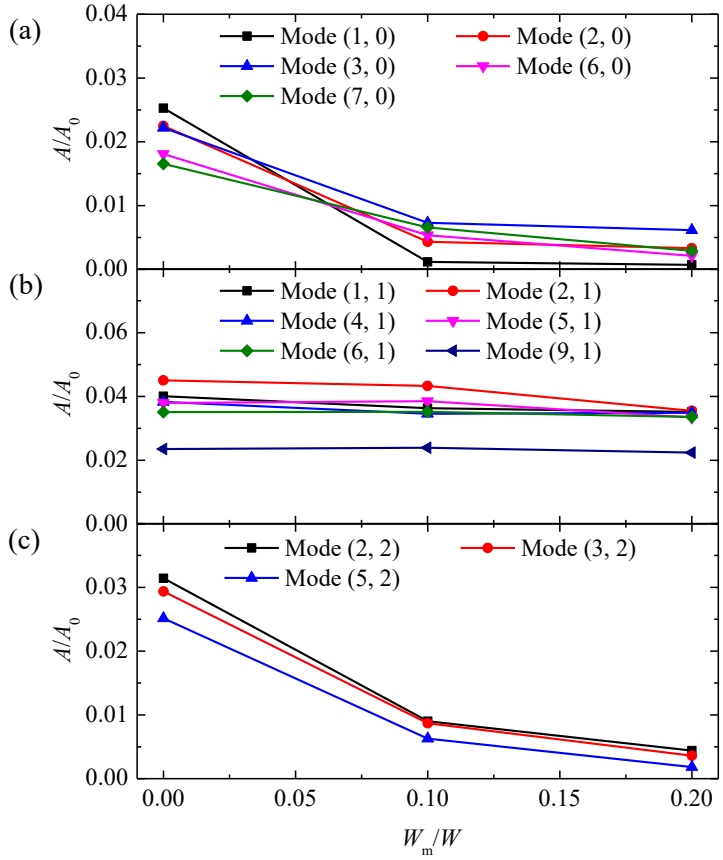

Fig. 16. Variation of the response amplitudes of different resonant modes at the corner (0, −12.5 m) excited by the water surface disturbance at the region A with respect to the width of harbor entrance under the conditions of A_0=0.3 m and that the center of harbor entrance is located at (100.0 m, 0): (a) five resonant modes with n=0; (b) six resonant modes with n=1; (c) three resonant modes with n=2.

Wang et al. (2011b) pointed out that small-scale seafloor movement usually induces small longitudinal oscillations, but evident larger transverse oscillations; evident longitudinal oscillations can be only induced by large-scale seafloor movements. Different from Wang et al. (2011b), it is clear that for the enclosed harbor studied in this paper (see Fig. 15a), small-scale water surface disturbance can induce not only remarkable combined-type oscillations [e.g. the modes (1, 1) and (2, 1)] but also notable purely longitudinal oscillations [e.g., the modes (1,0), (2, 0) and (3, 0)]. The

reason lies on that in Wang et al. (2011b), a harbor with fully opened entrance was studied, and the wave energy corresponding to longitudinal oscillations was rapidly radiated from the entrance. Hence, the small-scale seafloor movement usually induces weak longitudinal oscillations. On the contrary, for the enclosed harbor, the whole wave energy provided by the water surface disturbance is trapped inside the harbor, which causes that even a small-scale water surface disturbance can induce notable purely longitudinal oscillations. This explanation can be verified by the variation trend of the response amplitudes of the first type of eigenfrequencies with respect to the width of harbor entrance shown in Fig. 16a.

5.4. Effects of the location of harbor entrance

Fig. 17 shows the amplitude spectra of the time series of the free surface elevations at the corner (0, −12.5 m) excited by the water surface disturbances at the region A under the conditions of A_0=0.3 m, W_m=5.0 m and various locations of harbor entrance. Identical to Section 5.2.1, the lowest twenty eigenfrequencies are classified into the same four types, and only the first three types of eigenfrequencies are discussed in this section. For the first type of eigenfrequencies that correspond to the modes (m, n) with n=0, all their response amplitudes are small due to the significant wave leakage from the harbor. In addition, different locations of harbor entrance seem to have a negligible effect on them. For the second type of eigenfrequencies that correspond to the modes (m, n) with n=1, when the harbor entrance is located at the center of the right boundary of the harbor (i.e., x_m=100.0 m, y_m=0), their response amplitudes are all evident. However, as the location of harbor entrance deviates from the center of the right boundary, their amplitudes gradually decrease. For the third type of eigenfrequencies that correspond to the modes (m, n) with n=2, relatively large amplitudes appear when the centers of harbor entrance are at (100.0 m, ±5.0 m), while for the other three entrance locations, their amplitudes become very small.

To show these phenomena more intuitively, the variations of the response amplitudes of these three types of eigenfrequencies at the corner (0, −12.5 m) with respect to various locations of harbor entrance are shown in Fig. 18. Identical to Figs. 15 and 16, the reason why the response amplitudes of these three types of eigenfrequencies appear distinctly different variation trends with respect to various locations of harbor entrance also lies on the different relative positions of their node lines and antinode lines to the harbor entrance. For each of these resonant modes, when the center of

harbor entrance is superposed with one of the n+1 antinode lines, its wave energy is easier to leak from the entrance; in contrast, when the center of harbor entrance is overlapped with one of the n node lines, the wave energy leakage out of the harbor becomes much harder. It should be noted that the effect of the location of the harbor entrance on the oscillations was also investigated by Bellotti (2007). Different from the current study in which the resonance is induced by the water surface disturbance occurring inside the harbor, in Bellotti (2007), the harbor oscillations were excited by long waves propagating from the open sea. However, the phenomenon that the relative location of the node/antinode lines of resonant modes with respect to the harbor entrance greatly influences the wave energy exchange of the resonant mode between the harbor and the open sea was found by both of these two studies.

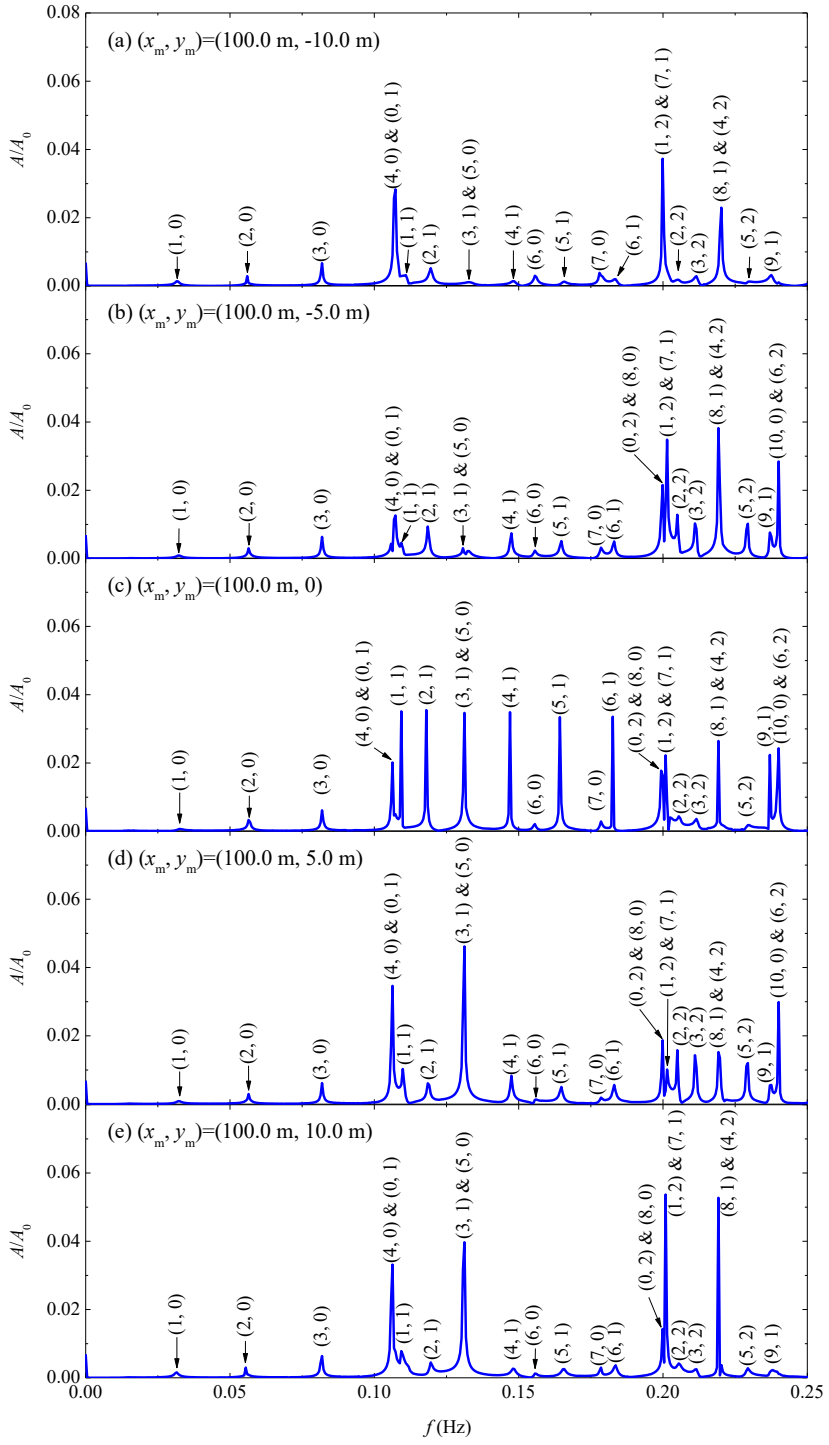

Fig. 17. Amplitude spectra of the time series of the free surface elevations at the corner (0, −12.5 m) excited by the water surface disturbances at the region A under the conditions of A_0=0.3 m, W_m=5.0 m and various locations of harbor entrance

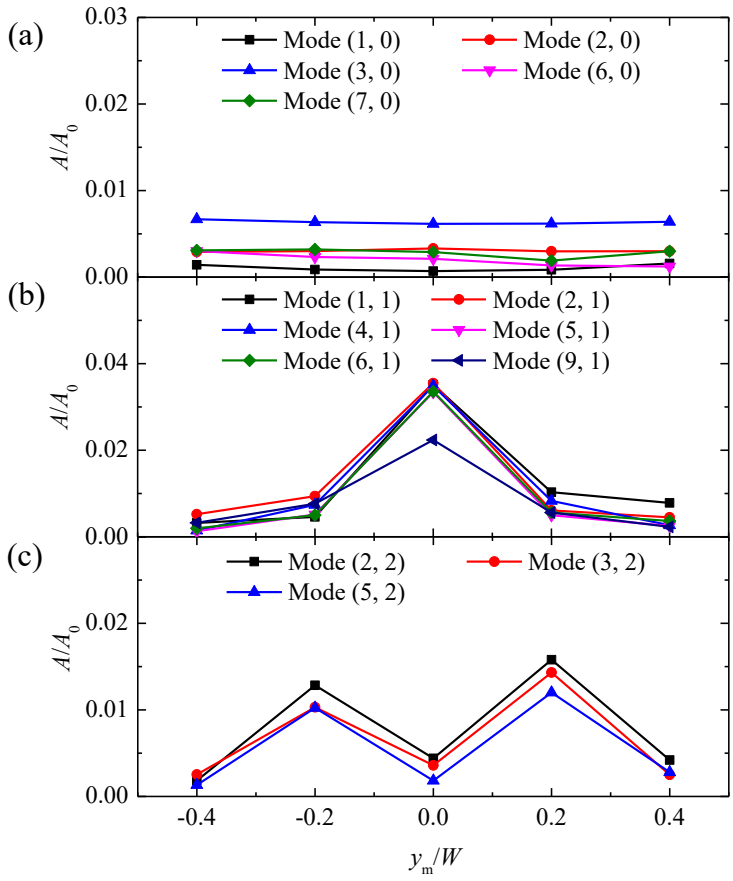

Fig. 18. Variation of the response amplitudes of different modes at the corner (0, −12.5 m) excited by the water surface disturbances at the region A with respect to the location of harbor entrance under the conditions of A_0=0.3 m and W_m=5.0 m: (a) five resonant modes with n=0; (b) six resonant modes with n=1; (c) three resonant modes with n=2.

6. Conclusions

Oscillations within an enclosed rectangular harbor and a set of partially opened rectangular harbors with various widths and locations of the entrance induced by cubic water surface disturbances with various initial heights and locations are simulated using the FUNWAVE 2.0 model. Different from Wang et al. (2011b), Shao et al. (2016) and Shao et al. (2017), the water depth inside and outside all the harbors is set to be constant. Effects of various initial heights and locations of the water surface disturbance and various widths and locations of the harbor entrance on the oscillations of different eigenfrequencies/modes are systematically investigated. The results of this study will improve the understanding of the harbor oscillations excited by external forcings occurring inside the harbor.

The following conclusions can be drawn from the results of the present study:

1. For both the enclosed harbor and the partially opened harbor, all the response amplitudes of various eigenfrequencies increase linearly with the initial height of the cubic water surface disturbance. This phenomenon may be attributed to that only small oscillations compared with the still water depth are investigated in current paper, and nonlinear energy transfers between different resonant components can be neglected.
2. The variation of the initial location of the water surface disturbance along the backwall of the harbor mainly affects the transverse oscillation pattern of various resonant modes. While the variation of the initial location of the water surface disturbance along the sidewall of the harbor mainly affects the longitudinal oscillation pattern of various modes.
3. The effects of the variation of the width of harbor entrance on the response amplitudes of various resonant modes depend on the relative positions of their node lines and antinode lines with respect to the harbor entrance. For the resonant modes with one of their node lines superposed with harbor entrance, their response amplitudes are not sensitive to the variation of the width of harbor entrance due to small difference on the wave energy levels inside and outside the entrance. On the contrary, for the resonant modes with one of their antinode lines overlapped with harbor entrance, their response amplitudes decrease sharply with the increasing of the entrance width due to large imbalance of the wave energy level around the entrance.
4. The influences of the location variation of harbor entrance on the response amplitudes of various resonant modes also depends on the relative positions of their node lines and antinode lines to the harbor entrance. For each resonant mode, when the harbor entrance is superposed with one of its antinode lines, its wave energy is easier to leak from the entrance, which causes a very small response amplitude inside the harbor. In contrast, when the harbor entrance is overlapped with one of its node lines, the wave energy leakage out of the harbor becomes much harder, which leads to a relatively larger response amplitude inside the harbor.

Finally, we reaffirm here that these conclusions are only valid for the enclosed rectangular harbor and the partially opened rectangular harbor with $W_m/W \leq 0.2$ when the relative initial height of the cubic water surface disturbance, A_0/h, is equal to or less than 0.1.

Acknowledgments

This work was financially supported by the National Natural Science Foundation of China (Grant no. 51609108), the Natural Science Foundation of the Jiangsu Higher Education Institutions of China (Grant no. 16KJB570004) and the Jiangsu Government Scholarship for Overseas Studies (awarded to Dr. Junliang Gao for study abroad at the University of Bath).

References

Bellotti, G., 2007. Transient response of harbours to long waves under resonance conditions. Coastal Engineering 54 (9), 680-693.

Bellotti, G., Briganti, R., Beltrami, G.M., 2012. The combined role of bay and shelf modes in tsunamis amplification along the coast. Journal of Geophysical Research 117, C08027, doi: 10.1029/2012JC008061.

Bowers, E.C., 1977. Harbour resonance due to set-down beneath wave groups. Journal of Fluid Mechanics 79, 71-92.

Chawla, A., Kirby, J.T., 2000. A source function method for generation of waves on currents in Boussinesq models. Applied Ocean Research 22 (2), 75-83.

Chen, G.-Y., Chien, C.-C., Su, C.-H., Tseng, H.-M., 2004. Resonance induced by edge waves in Hua-Lien Harbor. Journal of Oceanography 60, 1035-1043.

Chen, M.-Y., Mei, C.C., Chang, C.-K., 2006. Low-frequency spectra in a harbour excited by short and random incident waves. Journal of Fluid Mechanics 563, 261-281.

De Jong, M.P.C., Battjes, J.A., 2004. Seiche characteristics of Rotterdam Harbour. Coastal Engineering 51 (5-6), 373-386.

Dong, G., Wang, G., Ma, X., Ma, Y., 2010a. Harbor resonance induced by subaerial landslide-generated impact waves. Ocean Engineering 37 (10), 927-934.

Dong, G., Wang, G., Ma, X., Ma, Y., 2010b. Numerical study of transient nonlinear harbor resonance. Science China-Technological Sciences 53, 558-565.

Fabrikant, A.L., 1995. Harbor oscillations generated by shear flow. Journal of Fluid Mechanics 282, 203-217.

Gao, J., Ji, C., Gaidai, O., Liu, Y., 2016a. Numerical study of infragravity waves amplification during harbor resonance. Ocean Engineering 116, 90-100.

Gao, J., Ji, C., Gaidai, O., Liu, Y., Ma, X., 2017a. Numerical investigation of transient harbor

oscillations induced by N-waves. Coastal Engineering 125, 119-131.

Gao, J., Ji, C., Liu, Y., Gaidai, O., Ma, X., Liu, Z., 2016b. Numerical study on transient harbor oscillations induced by solitary waves. Ocean Engineering 126, 467-480.

Gao, J., Ji, C., Liu, Y., Ma, X., Gaidai, O., 2017b. Influence of offshore topography on the amplification of infragravity oscillations within a harbor. Applied Ocean Research 65, 129-141.

Gao, J., Ji, C., Liu, Y., Ma, X., Gaidai, O., 2018a. Numerical study on transient harbor oscillations induced by successive solitary waves. Ocean Dynamics 68 (2), 193-209.

Gao, J., Ji, C., Ma, X., Liu, Y., Gaidai, O., 2017c. Numerical investigation of infragravity wave amplifications during harbor oscillations influenced by variable offshore topography. Ocean Dynamics 67 (9), 1151-1162.

Gao, J., Ma, X., Dong, G., Wang, G., Ma, Y., 2016c. Numerical study of transient harbor resonance induced by solitary waves. Proceedings of the Institution of Mechanical Engineers, Part M: Journal of Engineering for the Maritime Environment 230 (1), 163–176.

Gao, J., Zhou, X., Zang, J., Chen, Q., Zhou, L., 2018b. Influence of offshore fringing reefs on infragravity period oscillations within a harbor. Ocean Engineering 158, 286-298.

Girolamo, P.D., 1996. An experiment on harbour resonance induced by incident regular waves and irregular short waves. Coastal Engineering 27, 47-66.

González-Marco, D., Sierra, J.P., Ybarra, O.F.d., Sánchez-Arcilla, A., 2008. Implications of long waves in harbor management: The Gijón port case study. Ocean & Coastal Management 51 (2), 180-201.

Kirby, J.T., Long, W., Shi, F., 2003. Funwave 2.0 Fully Nonlinear Boussinesq Wave Model On Curvilinear Coordinates. Report No. CACR-02-xx. Center for Applied Coastal Research, Dept. of Civil & Environmental Engineering, University of Delaware, Newark, Delaware.

Kofoed-Hansen, H., Kerper, D.R., Sørensen, O.R., Kirkegaard, J., 2005. Simulation of long wave agitation in ports and harbours using a time-domain Boussinesq model, Proceedings of the Fifth International Symposium on Ocean Wave Measurement and Analysis (WAVES), Madrid, Spain.

Kulikov, E.A., Rabinovich, A.B., Thomson, R.E., Bornhold, B.D., 1996. The landslide tsunami of November 3, 1994, Skagway Harbor, Alaska. Journal of Geophysical Research 101 (3), 6609-6615.

Kumar, P., Gulshan, 2017. Extreme wave-induced oscillation in Paradip Port under the resonance conditions. Pure and Applied Geophysics 174 (2), 4501-4516.

Kumar, P., Zhang, H., Kim, K.I., 2014. Spectral Density Analysis for Wave Characteristics in Pohang New Harbor. Pure and Applied Geophysics 171, 1169-1185.

Kumar, P., Zhang, H., Kim, K.I., Yuen, D.A., 2016. Modeling wave and spectral characteristics of moored ship motion in Pohang New Harbor under the resonance conditions. Ocean Engineering 119, 101-113.

López, M., Iglesias, G., 2014. Long wave effects on a vessel at berth. Applied Ocean Research 47, 63-72.

Losada, I.J., Gonzalez-Ondina, J.M., Diaz-Hernandez, G., Gonzalez, E.M., 2008. Numerical modeling of nonlinear resonance of semi-enclosed water bodies: Description and experimental validation. Coastal Engineering 55, 21-34.

Ma, Y., Chen, H., Ma, X., Dong, G., 2017. A numerical investigation on nonlinear transformation of obliquely incident random waves on plane sloping bottoms. Coastal Engineering 130, 65-84.

Mei, C.C., 1983. The Applied Dynamics of Ocean Surface Waves. Wiley, New York.

Mei, C.C., Agnon, Y., 1989. Long-period oscillations in a harbour induced by incident short waves. Journal of Fluid Mechanics 208, 595-608.

Okihiro, M., Guza, R.T., 1996. Observations of seiche forcing and amplification in three small harbors. Journal of Waterway, Port, Coastal and Ocean Engineering 122 (5), 232-238.

Rogers, S.R., Mei, C.C., 1978. Nonlinear resonant excitation of a long and narrow bay. Journal of Fluid Mechanics 88 (1), 161-180.

Shao, D., Feng, X., Feng, W., 2016. Numerical investigation of oscillations within a harbor of parabolic bottom induced by water surface disturbances. Applied Ocean Research 59, 153-164.

Shao, D., Feng, X., Feng, W., Hong, G., 2017. Numerical investigation of oscillations induced by submerged sliding masses within a harbor of constant slope. Applied Ocean Research 63, 49-64.

Vanoni, V.A., Carr, J.H., 1950. Harbor surging, Proceedings of the 1st International Conference on Coastal Engineering, Long Beach, pp. 60-68.

Wang, G., Dong, G., Perlin, M., Ma, X., Ma, Y., 2011a. An analytic investigation of oscillations

within a harbor of constant slope. Ocean Engineering 38, 479-486.

Wang, G., Dong, G., Perlin, M., Ma, X., Ma, Y., 2011b. Numerical investigation of oscillations within a harbor of constant slope induced by seafloor movements. Ocean Engineering 38 (17-18), 2151-2161.

Wang, G., Zheng, J., Liang, Q., Zhang, W., Huang, C., 2015. Theoretical analysis of harbor resonance in harbor with an exponential bottom profile. China Ocean Engineering 29 (6), 821-834.

Wang, G., Zheng, J., Liang, Q., Zheng, Y., 2014. Analytical solutions for oscillations in a harbor with a hyperbolic-cosine squared bottom. Ocean Engineering 83, 16-23.

Yalciner, A.C., Pelinovsky, E.N., 2007. A short cut numerical method for determination of periods of free oscillations for basins with irregular geometry and bathymetry. Ocean Engineering 34, 747-757.